Proceedings of the 21st ICSMGE, Vienna, Austria, 14 – 19 June 2026. Pistrol, Adam & Schweiger (eds.)
Published by: ÖGG, Austrian Society for Geomechanics, Salzburg, Austria, ISBN 978-3-9503898-4-5
https://doi.org/10.53243/ICSMGE2026-955

A 3D Numerical Investigation of Arching Mechanism Using Discrete Element Method (DEM)

Araz Salimnezhad, Mostafa Almasraf, Feyza Cinicioglu
Department of Civil Engineering, Ozyegin University, Istanbul, Turkey, feyza.cinicioglu@ozyegin.edu.tr

Behzad Soltanbeigi
Van Oord Dredging and Marine Contractors, Rotterdam, Netherlands

Ozer Cinicioglu
Department of Civil Engineering, Bogazici University, Istanbul, Turkey

ABSTRACT: The behavior and design of piled embankments constructed on soft soils are significantly influenced by soil arching, characterized by the redistribution of stresses between the yielding mass and the surrounding non-yielding soil. Understanding the micro-behavior of granular embankment fill and the interaction among embankment elements is crucial for comprehending the soil arching effect and load transfer mechanism in pile-supported embankments. Owing to the limitations of continuum mechanics, capturing the discrete interparticle interactions that occur during the formation or collapse of arches is not feasible. As a result, the arching mechanism can be reliably investigated through physical model experiments or Discrete Element Method (DEM) analysis. The trapdoor test serves as an experimental method to assess the arching phenomenon in granular materials. The plane strain and 3D model tests on DEM were constructed with a single trapdoor, similar to the Terzaghi trapdoor test concept. The heights were chosen as 7.5cm, 15cm, and 30cm to ensure the formation of all three main arching types of shear plane, partial, and full arching. To investigate the influence of boundary conditions, a series of partial arching models were developed under four distinct boundary configurations: (i) frictional boundary, (ii) frictionless boundary, (iii) periodic boundary in the x-direction (two-sided periodic), and (iv) periodic boundaries in both the x- and y-directions (four-sided periodic). Also, the arching efficiency was studied by calculating the Stress Reduction Ratios (SRR) for all models. The DEM was successfully able to capture the principal stress rotation as the main reason for the soil arching. Although reducing the computational time in DEM analyses, plane-strain models with a reduced out-of-plane depth should be applied with caution, as they may yield overly optimistic estimates of the SRR.

KEYWORDS: Granular materials, soil arching, trapdoor test, DEM analysis, stress reduction ratio, contact force chains.

1 INTRODUCTION

The Discrete Element Method (DEM) is commonly used to model the motion and interaction of individual grains. In DEM, granular materials are treated as collections of individual particles, with their positions, speeds, and the forces they exert on each other being tracked at very short time intervals (Cundall and Strack, 1979). Particle shape plays a crucial role in how particles interact, impacting their behavior at larger scales. Irregularly shaped particles tend to interlock, restraining their movement and altering the flow properties of the granular material.

In DEM simulations, different methods are used to account for particle shape. Most studies use spherical particles because they simplify contact detection and speed up simulations. A clump refers to a rigid body composed of overlapping spherical elements of varying diameters, functioning collectively as a single particle with a prescribed or arbitrary shape. In this study, irregular particle geometries were generated for the reconstruction of the actual morphology of typical crushed gravel particles. The geometry of particles plays a critical role in governing inter-particle friction and contact forces. Several studies (Stahl and Konietzky, 2011; Chen et al., 2012; Stahl et al., 2014; Indraratna et al., 2014; Miao et al., 2017) have employed clump-based approaches to simulate irregularly shaped particles across a range of applications. For this study, crushed limestone was chosen as the representative material, consistent with the laboratory investigations reported by Gao and Meguid (2018) and Chen et al. (2009).

Arching is a fundamental phenomenon in granular materials that occurs in a wide range of engineering applications, including the design of silos and hoppers, as well as geotechnical systems such as piled embankments, tunnels, and buried pipelines. As particles interact during flow through an opening or within a settling mass, arch-like structures develop, causing the pressure on the settling part to be reduced and the stresses to be redistributed within the granular material towards the stationary parts. Due to the nature of continuum mechanics, it is not possible to capture the discrete interparticle behavior occurring during the formation or collapse of the arches. Therefore, the study of the arching needs to be conducted using either physical model tests or DEM analyses. The trapdoor test serves as an experimental method to assess the arching phenomenon in granular materials. Terzaghi (1936) was the first to carry out trapdoor experiments, characterizing the arching effect as the mechanism of load transfer through granular materials. Numerous other researchers have conducted similar tests for various objectives (Chevalier et al., 2012; Costa et al., 2009; Vardoulakis et al., 1981). This highlights the need for further experimental research on arch formation in different scenarios.

2 NUMERICAL MODELING – DEM

2.1 *Materials and Methods*

The plane strain and 3D model tests on DEM were constructed with a single trapdoor (Figure 1), similar to the Terzaghi trapdoor test concept. The DEM model properties are given in Table 1. The trapdoor was lowered at a speed of 0.001 m/s. The heights were chosen as 7.5cm, 15cm, and 30cm. The mentioned fill heights were chosen to ensure the formation of all three main arching types of shear plane, partial, and full arching, (Lai et al., 2018). The trapdoor width was 7.5cm, and the out-of-plane width of the models was 10 cm. Also, the width of the stationary parts was 3.75cm. The range of motion for the trapdoor in the vertical (Z) direction was 5cm. In the 3D models, the stationary parts of the plane-strain model were modified as four square corner piles with a width of 3.75 cm.

The dimension of the 3D model in plan-view was a 0.15m by 0.15m square.

2.2 *The boundary effect and side physical walls*

To investigate the influence of boundary conditions and geometry–particle friction on trapdoor test results, a series of partial arching models were developed under four distinct boundary configurations: (i) frictional boundary, (ii) frictionless boundary, (iii) periodic boundary in the x-direction (two-sided periodic), and (iv) periodic boundaries in both the x- and y-directions (four-sided periodic). This will give an insight into the share of the loads from the weight of the hanging particles transferred to the side walls through the friction resistance. The hanging effect can be misleading in interpreting the arching evolution, considering the load redistribution results.

Comparing the force due to the weight of the particle column above the trapdoor with the force acting on the trapdoor obtained from EDEM, it was noticed that the boundary effect in the periodic boundary model is lower, and the arching is mostly due to particle-particle interaction. In the periodic boundary models, the depth of the models decreased from 10 cm to 3 cm. For the frictionless boundary models, the static and rolling friction coefficients were defined as zero, and the Hertz-Mindlin (No-slip) model with no rolling friction was selected.

Table 1. DEM model properties.

Parameter	Value
Density (particle) ρ [kg/m³]	2650
Coefficient of particle–particle friction μ_{pp}^{s}	0.56
Coefficient of particle–wall friction μ_{pw}^{s}	0.45
Coefficient of restitution (particle–particle), ε_p	0.15
Coefficient of restitution (particle–wall), ε_{pw}	0.5
Poisson ratio (particles), ν_p	0.25
Poisson ratio (wall), ν_w	0.25
Shear modulus (particles), G_p [Pa]	10^7
Shear modulus (wall), G_w [Pa]	10^{10}

2.3 *Setting linear periodic boundaries*

Using the Linear Periodic Boundaries, any particle leaving the domain in that direction will instantly re-enter it on the opposite side, which contributes to simulating an infinite medium.

Figure 2 illustrates the pressure over the trapdoor (obtained from hand calculation and EDEM) in four partial arching models, along with the elapsed calculation time of each analysis. However, the periodic boundary models have a smaller in-plane dimension compared to the physical boundary models (3cm compared to 10 cm); the hand-calculated total pressure over the trapdoor for all the models is almost the same.

The difference between the hand-calculated and EDEM-calculated pressure values over the trapdoor is due to the geometry-particle friction in the frictional physical boundary model. Due to the friction between the wall material and the particles, a share of the weight of the particles is conveyed to the side walls, which decreases the pressure over the trapdoor. Also, it can be observed from the force measurement (Figure 2). Therefore, it could be concluded that using the periodic boundary instead of the physical boundary could decrease the boundary effect without sacrificing the precision of the EDEM calculations.

The total number of particles, contacts total, and elapsed computation time for the plane-strain and 3D models with 7.5 cm, 15 cm, and 30 cm fill heights are given in Table 2. As shown in Table 2, the particle and contact numbers are considerably smaller than the physical boundary models due to the smaller depth of the model. This will be very important in decreasing the calculation time in the bigger and more complex DEM models.

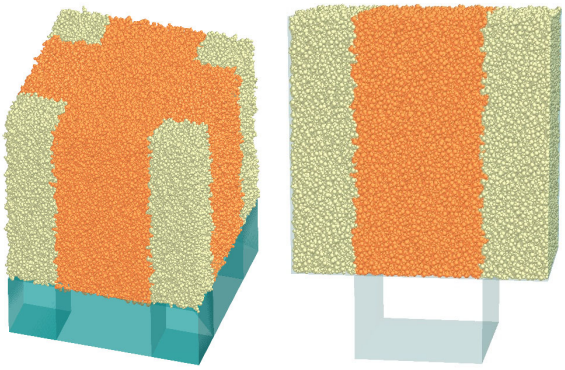

Figure 1. Plane-strain and 3D Partial arching models.

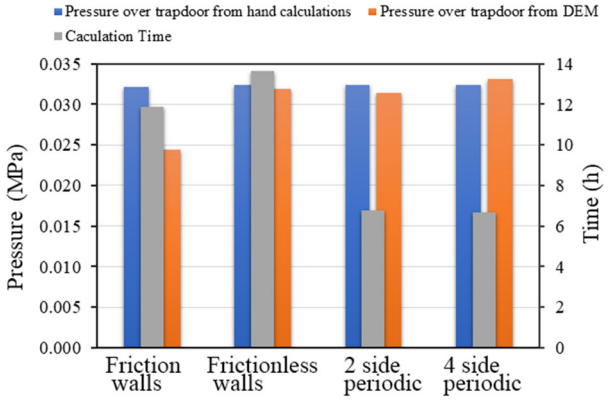

Figure 2. Pressure over the trapdoor in four partial arching models with the corresponding elapsed time of each analysis.

Table 2. Total number of particles, contacts, and elapsed time for plane-strain partial arching models.

Partial arching model analysis	Friction walls	Frictionless walls	Two-sided periodic	Four-sided periodic	3D periodic
Total number of particles	27580	27786	8341	8284	42662
Contacts total	90617	92081	27246	27335	139369
Elapsed computation time (h)	11.86	13.64	6.78	6.67	19.76

3 RESULTS AND DISCUSSIONS

For the partial arching cases in the plane strain models, when the fill height is 7.5 cm, the arching was not fully mobilized due to the insufficient fill height. The contact force chains above the subsoil rotate to a horizontal orientation (90° rotation) but do not overlap sufficiently to form an arch. Lowering the trapdoor changes the stress state of the fill, leading to settlements throughout the entire height of the fill. Also, the settlement of the soil at the surface of the model is almost equal to the range that the trapdoor is lowered ($\Delta S_{es} \approx \Delta S$) (Figure 3a). When the fill height increases to 15 cm (Figure 3b), the contact force chains above the subsoil act as arched force bridges that reach the surface (Figure 4a), causing partial arching. The forechain lines shown at the stationary parts suggest that the arches extend to the fill surface; therefore, the arch does not carry a noticeable burden. Thus, the arches are

less stable and important in efficient load transfer. However, in this case, the soil settlement at the surface is lower than the trapdoor motion range ($\Delta S_{es} < \Delta S$).

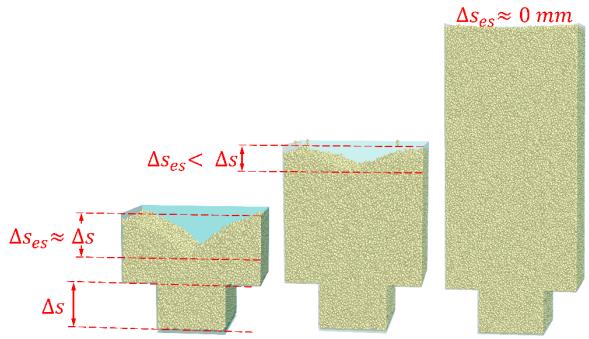

Figure 3. Particles' position at the end of the test for: a. shear plane arching; b. partial arching; c. full arching.

In a full arching case (the arching height is 30 cm) (Figure 3c), the direction of the contact force chains above the subsoil indicates that they rotate to a horizontal state at a specific height above the subsoil centerline, carrying the burden of the fill portion above the arch structure. So, no differential settlement could be seen at the surface of the soil ($\Delta S_{es} \approx 0$) (Figure 4c).

Figure 4 demonstrates the contact force chains at the end of the test for shear plane arching, partial arching, and full arching models. As is obvious in the model with 7.5 cm height (Figure 4a), the force-carrying chains (shown in red) are concentrated mostly above the trapdoor and within the settling soil mass. It is due to the insufficient height of the granular fill that causes the shear plane arching to rule. So, the force chains extending from the stationary parts could not reach each other to make a stable arch over the trapdoor.

For the model with a fill height of 15 cm (Figure 4b), a concentration of contact forces on the stationary side parts can be observed; however, complete unloading above the lowered trapdoor does not occur, resulting in differential settlement at the soil surface. Although force chains converge above the trapdoor to form an arch, the arch height is equal to the fill height, leaving no overlying burden for the arch to transfer to the stationary side parts (partial arching).

In contrast, for the model with a fill height of 30 cm (Figure 4c), the contact forces are clearly concentrated on the stationary side parts. The unloading above the lowered trapdoor is evident (indicated by the white zones), and no differential settlement develops at the soil surface (full arching).

In this case, the force chains converge above the trapdoor to form an arch, and the greater fill height provides sufficient overburden for the arch to transfer the load effectively to the stationary side parts.

Figure 5 illustrates the normal contact forces in the horizontal (x) direction. It shows that the lateral forces inside the soil make an arched-shaped structure. The difference between blue and red colors is due to the different alignment of the forces, which causes them to be placed in positive or negative signs. The normal forces in the x direction also show the concept of increased lateral earth pressure coefficient and the clogging effect over the trapdoor.

There are several methods to measure the load transformation efficiency in piled-supported embankments or in arching physical experiments. The arching efficiency described by the Stress Reduction Ratios (SRR) is defined as the ratio of the average pressure on the trapdoor at a certain settlement to the initial pressure on the trapdoor at zero settlement and it depends on the fill properties (density, internal friction angle, etc.), acting loads (static, cyclic, different-phase cyclic) and model geometry (fill height, trapdoor width, stationary parts width, and the ratio of the fill height to the stationary parts spacing).

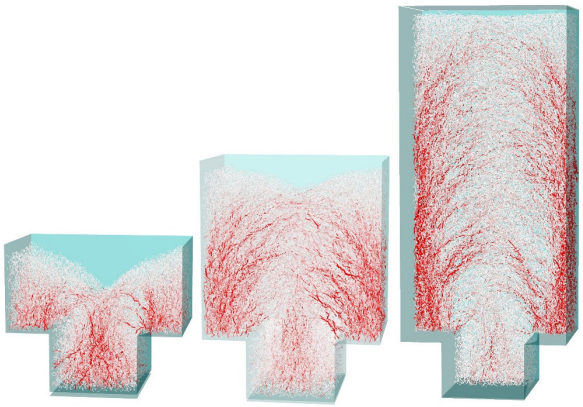

Figure 4. Contact force chains at the end of the test for: a. shear plane arching; b. partial arching; c. full arching.

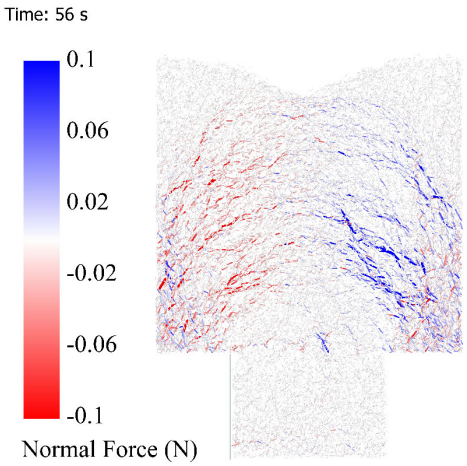

Figure 5. Normal contact force in the x direction for the partial arching model.

Figure 6 depicts the stress reduction ratio for the shear-plane, partial, and full arching models versus the analysis time. It could be understood that at the first stage, which is related to the filling of the box setup, the SRR increases and reaches the maximum possible value (1). At the end of the filling stage, the trapdoor was lowered to start the arching monitoring phase. At the onset of trapdoor lowering, a sudden and tremendous decrease in SRR could be seen, which is due to the unloading effect following the downward movement of the trapdoor.

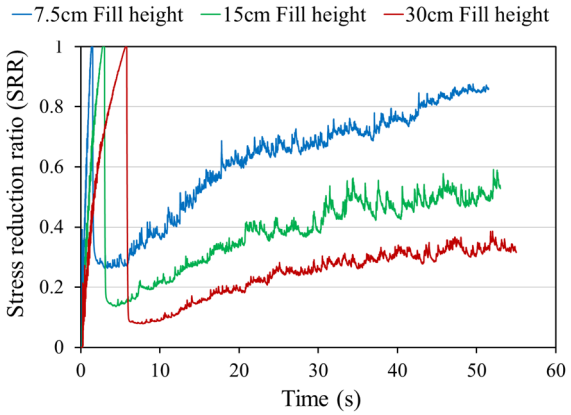

Figure 6. Stress reduction ratio for the plane strain arching models.

As the test proceeded and the trapdoor was lowered further, some share of the unloaded pressure over the trapdoor was recovered. It happened due to the large displacement of the soil particles following the further displacement of the trapdoor, which led to the destruction and the generation of less efficient arches. As expected, the greatest reduction in SRR values was associated with full arching, followed by partial arching and shear-plane arching, respectively. In the full arching model, the largest amount of the loads is transferred to the side stationary parts at the end of the test.

Figure 7 depicts the stress reduction ratio for the 3D, partial, and full arching models versus the analysis time. The difference in the filling time is related to the volume of the models, as the full arching model with a height of 0.3m took a longer time to be filled with the particles. However, the areas of the piles' surfaces in the 3D models are smaller than the area of the stationary parts of the plane-strain model; 3D models exhibit a better performance regarding the SRR, showing a more efficient load transfer to the piles. As expected, the greatest reduction in SRR values was associated with full arching, followed by partial arching and shear-plane arching, respectively. In the full arching model, the largest amount of the loads is transferred to the side stationary parts at the end of the test.

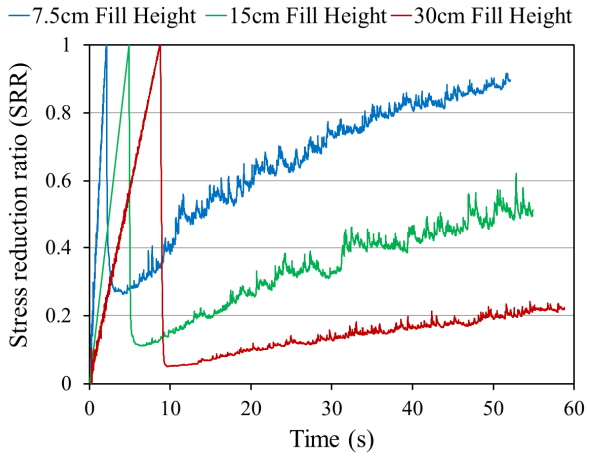

Figure 7. Stress reduction ratio for the 3D arching models.

Figure 8 demonstrates the SRR variation by time for the partial arching models with frictional physical boundaries, frictionless physical boundaries, periodic boundaries in the X direction, and periodic boundaries in the X and Y directions.

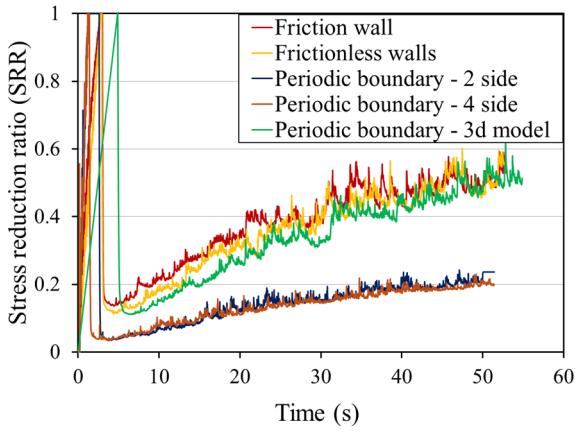

Figure 8. Stress reduction ratio variation by time for the plane-strain and 3D partial arching models.

The modelling concept and approach are different for the plane-strain and 3D cases; the SRR pattern of the 3D model is similar to the SRR curve of the plane-strain models. Although reducing the computational time in DEM analyses, plane-strain models with a reduced out-of-plane depth should be applied with caution, as they may yield overly optimistic estimates of the SRR. It happens due to limitations that the thin out-of-plane dimension dictates to the arch formation and evolution.

4 CONCLUSIONS

This study investigated soil arching in trapdoor models using DEM, focusing on the effects of boundary conditions, fill height, and dimensionality on arch formation and efficiency. The key findings are:

- Arching mobilization depends strongly on fill height: shallow fills (7.5 cm) lead to shear-plane arching with surface settlements, intermediate fills (15 cm) produce unstable partial arches, and greater fills (30 cm) achieve full arching with efficient load transfer and negligible settlement.
- Stress Reduction Ratio (SRR) analysis confirms that full arching transfers the largest share of loads to stationary parts, though it also shows the greatest SRR reduction during trapdoor lowering, and a sufficient fill height is needed for the formation of full arch.
- 3D models exhibit more efficient load transfer to piles than plane-strain models, highlighting the need for caution when applying reduced-depth plane-strain approaches, which may overestimate SRR.

5 ACKNOWLEDGEMENTS

The authors would like to thank the Scientific and Research Council of Turkey (TUBITAK) for supporting this study with project number 122M040.

6 REFERENCES

Cundall, P.A., and Strack, O.D.L. 1979. A discrete numerical model for granular assemblies. *Géotechnique*, 29(1), 47–65.

Chen, C., McDowell, G.R., and Thom, N.H. 2012. Discrete element modelling of cyclic loads of geogrid-reinforced ballast under confined and unconfined conditions. *Geotextiles and Geomembranes*, 35, 76–86.

Stahl, M., Konietzky, H., Te Kamp, L., and Jas, H. 2014. Discrete element simulation of geogrid-stabilised soil. *Acta Geotechnica*, 9(6), 1073–1084.

Stahl, M., and Konietzky, H. 2011. Discrete element simulation of ballast and gravel under special consideration of grain-shape, grain-size and relative density. *Granular Matter*, 13(4), 417–428.

Indraratna, B., Ngo, N.T., Rujikiatkamjorn, C., and Vinod, J.S. 2014. Behaviour of fresh and fouled railway ballast subjected to direct shear testing: discrete element simulation. *International Journal of Geomechanics*, 14(1), 34–44.

Miao, C.X., Zheng, J.J., Zhang, R.J., and Cui, L. 2017. DEM modelling of pull-out behaviour of geogrid-reinforced ballast: the effect of particle shape. *Computers and Geotechnics*, 81, 249–261.

Gao, G., and Meguid, M.A. 2018. Effect of particle shape on the response of geogrid-reinforced systems: insights from 3D discrete element analysis. *Geotextiles and Geomembranes*, 46(6), 685–698.

Chen, Q., Abu-Farsakh, M., and Sharma, R. 2009. Experimental and analytical studies of reinforced crushed limestone. *Geotextiles and Geomembranes*, 27(5), 357–367.

Lai, H.J., Zheng, J.J., Zhang, R.J., and Cui, M.J. 2018. Classification and characteristics of soil arching structures in pile-supported embankments. *Computers and Geotechnics*, 98, 153–171.

Terzaghi, K. 1936. Stress distribution in dry and in saturated sand above a yielding trap-door.